# A variation on the Chamberlin trimetric map projection

Author: author@email.com, 55 XXXXXX St, XXXXXXXX, XX, 01234

**ARTICLE HISTORY**
Compiled February 9, 2021

**ABSTRACT**
A variation of the Chamberlin trimetric map projection is presented, termed the matrix trimetric projection. The matrix trimetric projection amounts to a linear transformation of the squares of the distances between a given point and three control points. The formula of the forward projection is simpler than the Chamberlin projection, making it nearly twice as fast to calculate. The matrix trimetric projection has an inverse formula requires numerical iteration of only one parameter. Comparisons between the two projections are made using a representative list of control points. The Chamberlin trimetric projection outperforms the matrix trimetric projection on measures of angle deformation and scale deformation, but the reverse is true for a measure of distance deformation, and the difference between the results of the projections is small. Considered all together, the matrix trimetric projection is a viable alternative for the use cases of the Chamberlin trimetric projection.

*Keywords: Chamberlin trimetric, matrix trimetric, projection, cartography, distortion, distance, triangulation*

## 1. Introduction

Any map projection must introduce some form of distortion. In particular, no map projection can be both conformal (angle-preserving) and equal-area. Projections that eliminate one form of distortion often introduce a great deal of another form of distortion. For example, many conformal projections drastically enlarge some areas compared to others, most notoriously the Mercator projection, but also the stereographic and the Lambert conformal conic projections. (Snyder, 1987) A compromise map projection is one that seeks to balance different kinds of distortion; allowing small amounts of different kinds of distortion can produce a map that is more aesthetically pleasing.

The Chamberlin trimetric projection (CTP) is such a compromise map projection. It is named for Wellman Chamberlin, a chief cartographer for the National Geographic Society, which has published wall and atlas maps using his projection. The CTP is appropriate for mapping whole continents and large portions of continents. (Christensen, 1992) It may be thought of as a form of triangulation. Most often, the CTP is used with the spherical approximation of the Earth. Being a compromise projection, the CTP does not perfectly preserve angle, area, or distance. For most practical ellipsoids, distortions due to the spherical approximation are negligible compared to distortions due to the projection itself.

The CTP is based on a simple geometric construction, using three arbitrary points on the sphere called the control points. Algebraic formulas are preferred for modern computerized GIS, and the formulas for the CTP are somewhat involved. This is pre-

sented in Christensen (1992), and can be seen in the source code to its implementation in PROJ contributors (2019); the algorithmic form has branching logic depending on where the given point lies with respect to the geodesics between control points, and when the given point lies near a control point.

This text presents a new map projection called the matrix trimetric projection (MTP) as an alternative to the CTP. A geometric construction related to the CTP results in a map projection that is similar but has a simpler formula. This formula is a closed-form matrix function of the squares of the distances, and allows for a tractable inverse. As the derivations involve matrices and linear algebra, refer to a text such as Strang (1980) if needed.

## 2. Preliminaries

These projections will almost always be implemented using the spherical approximation, so formulas for that approximation are given shortly, and we'll refer to "the sphere" instead of "the ellipsoid". That said, the forward formulas for the CTP and MTP are agnostic of the surface to be projected, depending only on the result of the distance function.

Points on the sphere are denoted $\mathbf{v}$ or subscripted versions. $\mathbf{v}$ is a 3-vector with unit length, such that it lies on the unit sphere. Using this vector form allows us to take advantage of linear algebra. Points specified by latitude $\varphi$ and longitude $\lambda$ can be converted to a unit vector as so:(Lapaine, 2017)

$$\mathbf{v} = \begin{bmatrix} x \\ y \\ z \end{bmatrix} = \begin{bmatrix} \cos(\varphi)\cos(\lambda) \\ \cos(\varphi)\sin(\lambda) \\ \sin(\varphi) \end{bmatrix}. \tag{1}$$

The reverse conversion is:

$$\begin{aligned} \varphi &= \arctan\left(\frac{z}{\sqrt{y^2 + x^2}}\right), \\ \lambda &= \arctan\left(y, x\right), \end{aligned} \tag{2}$$

where the 2-variable form of arctan, commonly called `arctan2` or `atan2` in numeric software libraries, is used for $\lambda$.

One statement of the distance function on the sphere is

$$d\left(\mathbf{v}_i, \mathbf{v}_j\right) = R \arccos\left(\mathbf{v}_i \cdot \mathbf{v}_j\right) \tag{3}$$

where $R$ is the radius of the Earth. There are equivalent functions in terms of vectors that are more numerically stable for certain range of arguments, but this is the form used in the derivations.

Points in the Euclidean plane are denoted by $\mathbf{p} = [x, y]$ and subscripted versions. Planar distances are found using the usual Euclidean norm: $\|\mathbf{p}_a - \mathbf{p}_b\|$.

Let $\mathbf{v}_1$, $\mathbf{v}_2$, $\mathbf{v}_3$ be control points on the sphere, in counter-clockwise order, and let $\mathbf{V}$ be the matrix having $\mathbf{v}_i$ as its $i$th column. Let $\mathbf{p}_1$ etc. be the control points on the plane, in corresponding order, and $\mathbf{P}$ be the matrix having $\mathbf{p}_i$ as its $i$th column. The triangles with vertices at $\mathbf{v}_i$ or $\mathbf{p}_i$ are called the control triangles: spherical or planar

control triangle, respectively, if the distinction is important. For this paper, very small triangles are excluded, as are triangles with areas of an entire hemisphere or more; neither are typical use cases for the CTP. Note that the planar control triangle is **not** the image of the spherical control triangle under either projection! That image is slightly larger, containing the planar control triangle, and has curved edges.

For both projections, $\mathbf{p}_i$ must be arranged such that $d(\mathbf{v}_i, \mathbf{v}_j) = \|\mathbf{p}_i - \mathbf{p}_j\|$ for all $i$ and $j$ in $\{1, 2, 3\}$: the spherical length of the edges of the spherical control triangle are equal to the Euclidean lengths of the planar control triangles. Without loss of generality, also assume that $\|\mathbf{p}_i\|$ is the same for all $i$, such that the circumcenter of the control triangle lies at the origin. This just removes a translation in the plane in order to simplify the formula for the MTP; false northing and easting can be added later. Given $\mathbf{v}_i$, $\mathbf{p}_i$ can be constructed as follows. Let $i, j, k$ be a cyclic permutation of $\{1, 2, 3\}$, and let $s_k = d(\mathbf{v}_i, \mathbf{v}_j)$, such that side $k$ with length $s_k$ is opposite point $k$. The circumradius of the Euclidean triangle with sides of length $s_k$ is (Isaacs, 2009)

$$C = \frac{\prod_i s_i}{\sqrt{\sum_i 2s_i^2 s_{i+1}^2 - s_i^4}}. \tag{4}$$

From the (Euclidean) law of cosines, the interior angle $\phi_i$ at each vertex is

$$\phi_i = \arccos\left(\frac{s_k^2 + s_j^2 - s_i^2}{2s_k s_j}\right). \tag{5}$$

Then a set of points satisfying the requirements are given as so:

$$\mathbf{P} = \begin{bmatrix} C\cos(2\phi_2) & C\cos(2\phi_1) & C \\ C\sin(2\phi_2) & -C\sin(2\phi_1) & 0 \end{bmatrix}. \tag{6}$$

These points can be rotated about the origin as desired. Note that some intermediate values in Equation 4 may be large. This should not cause a problem on modern computers using common geographic units of distance, but some special applications may need to scale these values to avoid overflow.

## 3. Forward projection

Figure 1 shows the geometric construction of the CTP and the MTP. We start with the CTP. Let $\mathbf{v}$ denote the point to project, and let $r_i = d(\mathbf{v}_i, \mathbf{v})$ be the true distances from each control point to $\mathbf{v}$. On the sphere, Figure 1a shows the control triangle with vertices $\mathbf{v}_i$, the given point $\mathbf{v}$, and circles of radius $r_i$ centered on $\mathbf{v}_i$ and passing through $\mathbf{v}$. Moving to the plane, Figure 1b shows circles of the same radius $r_i$ centered on $\mathbf{p}_i$. The circles appear to all intersect at a single point, but due to the difference in curvature between the sphere and the plane they in fact form a small triangle with curved edges, as shown in Figure 1c. In the time of manual plotters the exact definition of this point was less important, but Christensen (1992) and modern implementations (e.g. PROJ contributors, 2019) use the centroid of the small triangle, denoted $\mathbf{p}_c$. Note that each pair of circles intersects in (at most) two points, so the algorithm must choose which point makes up the small triangle. In Christensen (1992) this is done

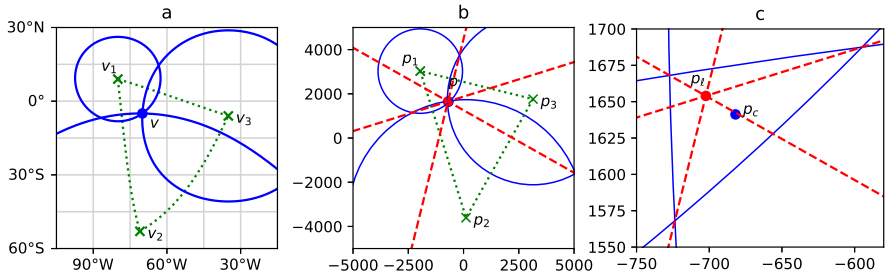


**Figure 1.** Construction of the CTP and MTP. Plot 1a is in equirectangular projection. Plot 1b is the projection to the plane. Plot 1c is the same as plot 1b, zoomed in to the small triangle created by the three circles. $\mathbf{p}_c$ is the point projected by the CTP and $\mathbf{p}_m$ is the point projected by the MTP. Green solid lines indicate the control triangles, the circles are blue dots, and the perpendiculars are red dashes.

by comparing the azimuths between each pair of control points to the azimuths from each control point to the given point.

Construction of the MTP starts like the CTP. If one draws a line through the two points of intersection of each pair of circles, that line is perpendicular to the triangle edge. These are the dashed red lines in Figure 1b and c. The three lines, one for each pair of circles, appear to meet at a single point; this observation can be proven with a simple triangle theorem sometimes attributed to Carnot. (Posamentier & Salkind, 1996; Wohlgemuth, 2010) This point is denoted $\mathbf{p}_m$. For most points within the control triangle $\mathbf{p}_m$ lies within the small triangle, although this is not true in general and is not necessary to create a valid map projection. (If $\mathbf{v}$ lies on a control triangle edge, one pair of circles has a single point of intersection. One can draw a perpendicular through that point of intersection and continue as in the general case.)

The equations of each perpendicular line, taken together, create a linear system. It is an overdetermined system of 3 equations in 2 variables, but since all 3 lines meet at the same point, it has a solution. Ultimately this system can be solved for $\mathbf{p}_m$ to define a forward map projection as follows.

$$\mathbf{p}_m = \mathbf{M} \begin{bmatrix} r_1^2 & r_2^2 & r_3^2 \end{bmatrix}^\top, \tag{7}$$

$$\mathbf{M} = \frac{1}{2T} \begin{bmatrix} y_3 - y_2 & y_1 - y_3 & y_2 - y_1 \\ x_2 - x_3 & x_3 - x_1 & x_1 - x_2 \end{bmatrix} = \frac{1}{2T} \begin{bmatrix} 0 & -1 \\ 1 & 0 \end{bmatrix} \mathbf{P} \begin{bmatrix} 0 & -1 & 1 \\ 1 & 0 & -1 \\ -1 & 1 & 0 \end{bmatrix}, \tag{8}$$

$$T = \begin{vmatrix} x_1 & x_2 & x_3 \\ y_1 & y_2 & y_3 \\ 1 & 1 & 1 \end{vmatrix}. \tag{9}$$

$T$ is equal to twice the area of the Euclidean control triangle.

The matrix $\mathbf{M}$ has a (right) nullspace spanned by the vector $[1, 1, 1]^\top$. This implies the MTP is not one-to-one for all possible values of $r_i$. For example, for any values of $r_i$ such that $r_1 = r_2 = r_3$, then $\mathbf{p}_m = [0, 0]^\top$. The CTP and MTP project the entire sphere to a bounded portion of the plane; the boundary of that portion can be termed the boundary of the projection. There is a region of overlap that is mapped into the

same area but in reverse orientation. That region includes the antipodes of the control points. In real applications, the overlap region of the sphere can be excluded.

## 4. Inverse projection

Given $\mathbf{p}_m$, start to invert the projection as so:

$$\begin{bmatrix} k_1 & k_2 & k_3 \end{bmatrix}^\top = \mathbf{M}^+ \mathbf{p}_m \,, \tag{10}$$

$$\mathbf{M}^+ = \frac{2}{3} \begin{bmatrix} -2x_1 + x_2 + x_3 & -2y_1 + y_2 + y_3 \\ x_1 - 2x_2 + x_3 & y_1 - 2y_2 + y_3 \\ x_1 + x_2 - 2x_3 & y_1 + y_2 - 2y_3 \end{bmatrix} = \frac{2}{3} \begin{bmatrix} -2 & 1 & 1 \\ 1 & -2 & 1 \\ 1 & 1 & -2 \end{bmatrix} \mathbf{P}^\top . \tag{11}$$

$k_i = r_i^2 - h$ for some value of the free parameter $h$. This is a general solution to inverting Equation 7; $\mathbf{M}^+$ is the pseudoinverse of $\mathbf{M}$ and vice versa. Because $\mathbf{M}^+$ has a left nullspace spanned by the vector $[1, 1, 1]$, it follows that $\sum_i k_i = 0$, and then that $h = \frac{1}{3} \sum_i r_i^2$. These equations are not enough to determine $r_i$ and $\mathbf{v}$; information about the sphere needs to be introduced.

To simplify the derivation, use $R = 1$, such that distance on the surface of the sphere has units of radians of arc. The circle of points $\mathbf{v}$ at distance $r_i$ from a point $\mathbf{v}_i$ is simply the circle created by a plane intersecting the sphere. Rearranging the distance function, this plane may be specified as $\mathbf{v}_i \cdot \mathbf{v} = \cos(r_i)$. These planes combined together give a linear system. Thus,

$$\mathbf{v} = \mathbf{V}^{-1} \begin{bmatrix} \cos(r_1) & \cos(r_2) & \cos(r_3) \end{bmatrix}^\top . \tag{12}$$

For the point to lie on the unit sphere, $\|\mathbf{v}\| = 1$. Let $\mathbf{c}$ be a vector with $i$th component $\cos(r_i)$. Then, $\mathbf{c}^\top \left(\mathbf{V}^\top \mathbf{V}\right)^{-1} \mathbf{c} = 1$. Make the substitution

$$r_i = \sqrt{k_i + h} \,. \tag{13}$$

We now have an equation with one unknown, $h$.

Some obvious bounds can be placed on $h$. In units of radians, $0 \leq r_i \leq \pi$. Since this must hold for every $r_i$, it follows that

$$h_{\min} = -\min_i k_i \leq h \leq \pi^2 - \max_i k_i = h_{\max} \,. \tag{14}$$

Within these bounds, there may be at most two solutions for $h$. The solution with smaller $h$ is the desired one, and the one with larger $h$ corresponds to the overlap region.

Let $\mathbf{A} = \left(\mathbf{V}^\top \mathbf{V}\right)^{-1}$ and

$$f(h) = \mathbf{c}^\top \mathbf{A} \mathbf{c} - 1 \,. \tag{15}$$

The derivative of $f(h)$ is

$$f'(h) = -\mathbf{c}^\top \mathbf{A} \mathbf{b} \,, \tag{16}$$

| Region | Point | | | Side length | | | Area |
|---|---|---|---|---|---|---|---|
| | 1 | 2 | 3 | 1 | 2 | 3 | |
| Africa Wall | 19°3'W, 24°25'N | 20°E, 35°S | 59°3'E, 24°25'N | 7,783 | 7,785 | 7,783 | 32.38 |
| North America Wall | 150°W, 55°N | 92°30'W, 10°N | 35°W, 55°N | 7,064 | 6,434 | 7,064 | 23.71 |
| South America Wall | 80°W, 9°N | 71°W, 53°S | 35°W, 6°S | 6,161 | 5,259 | 6,947 | 17.70 |
| Europe Wall | 15°E, 72°N | 8°W, 33°N | 38°E, 33°N | 4,254 | 4,541 | 4,541 | 9.09 |
| E South America | 63°33'W, 8°8'N | 58°33'W, 34°35'S | 35°13'W, 5°47'S | 4,000 | 3,502 | 4,779 | 7.25 |
| S South America | 43°W, 18°S | 72°W, 18°S | 72°W, 56°S | 4,225 | 4,874 | 3,064 | 6.77 |
| Australia | 134°E, 8°S | 110°E, 32°S | 158°E, 32°S | 4,487 | 3,643 | 3,643 | 6.76 |
| NW South America | 69°W, 25°S | 55°W, 10°N | 85°W, 10°N | 3,284 | 4,261 | 4,177 | 6.70 |
| Canada Wall | 150°W, 60°N | 97°30'W, 50°N | 45°W, 60°N | 3,423 | 5,197 | 3,423 | 6.11 |
| Canada Atlas | 98°13'W, 61°39'N | 135°W, 40°N | 55°W, 40°N | 6,560 | 3,761 | 3,449 | 5.28 |

**Table 1.** Table of control triangles and their measurements, from Christensen (1992). Side $n$ is opposite point $n$. Lengths are in km, and areas are in millions of square km. Measurements use spherical approximation.

where $\mathbf{b}$ is a vector with $i$th component $\operatorname{sinc}\left(\sqrt{k_i + h}\right)$. Note that $f'(h)$ and $f(h)$ share many of the same terms, which can be exploited for more efficient calculation. Given all the preceding, Newton's method can be applied to solve for $h$. A suitable initial condition is $h = h_{\min}$, which satisfies $f(h) = 0$ at the control points. This initial condition consistently results in convergence to the lower root of $f(h)$.

The error is roughly proportional to the final value of $|f(h)|$. A stopping condition of $|f(h)| < 10^{-4}$ results in an accuracy of 1 meter or better. For points in or near the control triangle, this condition is met in only a few iterations. Convergence is somewhat slower farther away from the control triangle. At the boundary of the projection, the lower solution and upper solution are the same and $f(h) = f'(h) = 0$ so Newton's method converges at a merely linear rate. (Burden & Faires, 2006)

## 5. Comparison

The open-source C++ package PROJ (PROJ contributors, 2019) contains an implementation of the CTP. We implemented the MTP as a patch to PROJ, to enable a fair comparison of computation time, and to take advantage of the existing framework.

Christensen (1992) gave a list of control triangles for the CTP in that paper's Table 1. The control triangles are repeated in this text's Table 1. These serve as a set of test cases for comparing the CTP and MTP. The length of each side and the area of each triangle (with the spherical approximation given earlier) is also given, and the control triangles are sorted by area.

To measure distortion of area and angle, we use the areal scale factor $s$ and max-

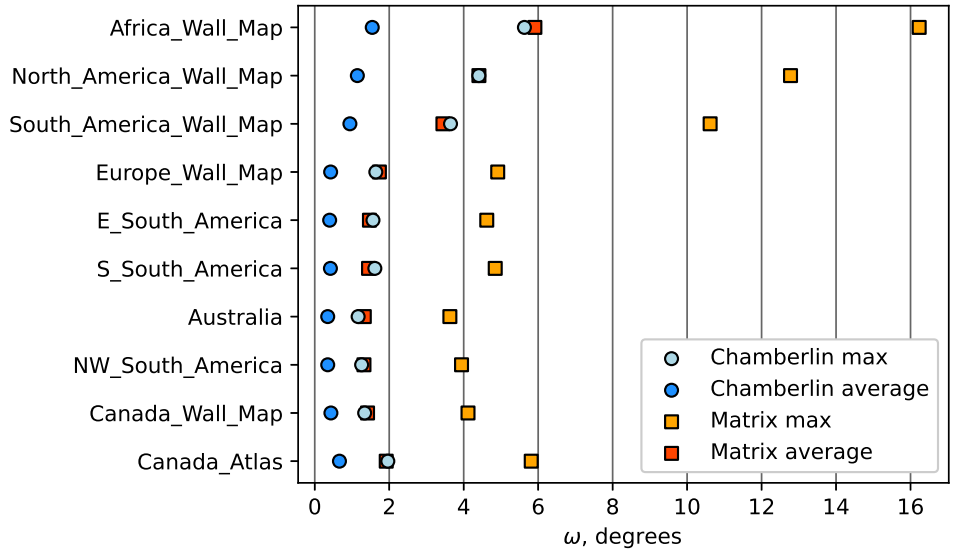


**Figure 2.** Comparison of maximum angular deformation $\omega$.

imum angular deformation $\omega$ as defined in equations 12–15, 27, and 28 in section 4 of Snyder (1987). These are implemented in the `proj_factors()` function of PROJ, which estimates the derivatives numerically. There is no standard measurement of distance distortion for map projections, but for the projections in this text it makes sense to measure distances from the control points. Let $r_i = d(\mathbf{v}_i, \mathbf{v})$ be the distance from $\mathbf{v}_i$ to $\mathbf{v}$ on the sphere, as earlier, and let $\ell_i = \|\mathbf{p}_i - \mathbf{p}\|$ be the distance from $\mathbf{p}_i$ to $\mathbf{p}$ in the plane. Our new measure, the total distance deviation or $D$, is the sum of differences in the distances measured on projected and unprojected distances:

$$D = \sum_i |r_i - \ell_i| \,. \tag{17}$$

We use the spherical approximation to the Earth, with a radius of 6,371 km, approximately equal to the most common mean radii. (Snyder, 1987)

For each spherical control triangle, summary statistics for $\omega$, $D$, and $s$ are shown in Figures 2–4. Note that the control triangles are sorted by area in these figures as well. These statistics are measured within the spherical control triangles, and should not be taken to summarize the entire map; in most cases, the region of interest extends outside the triangle. Rather, the statistics allow a quantitative comparison of the two projections.

As shown in Figure 2, the MTP consistently has a larger $\omega$ than the CTP; in fact, the maximum $\omega$ for the CTP is near the average $\omega$ for the MTP. Maximum and average $\omega$ trend upwards with control triangle area, although asymmetry of the control triangle has some influence too, as in the Canada triangles. The maximum $\omega$ for the MTP is about 3 times that for the CTP, and the average $\omega$ is about 3 to 4 times. However, for moderately-sized triangles, the maximum $\omega$ values are small for both projections, not exceeding 6°. Even for the large triangles – Africa, North America, and South America Wall Maps – the maximum distortion is tolerable, and

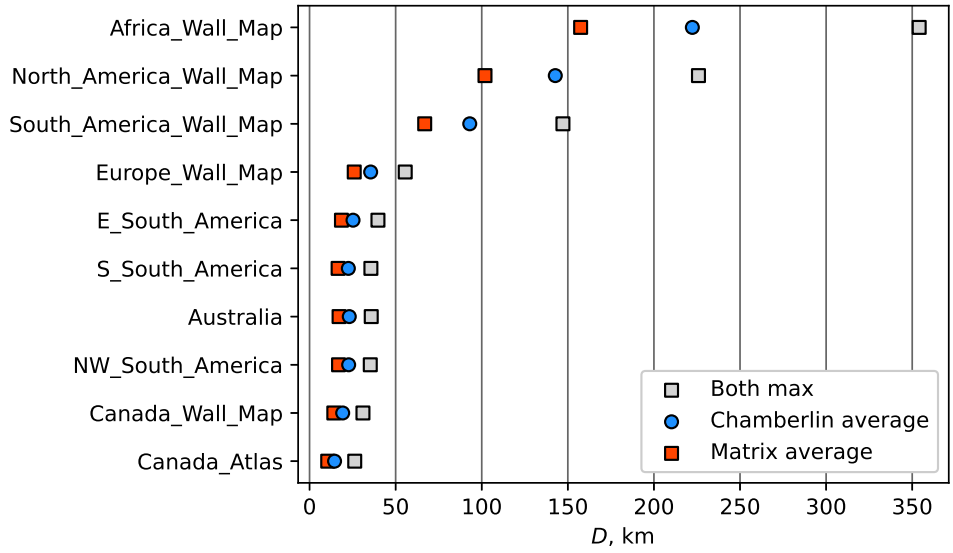


**Figure 3.** Comparison of total distance deviation $D$.

the average does not exceed 6°.

Total distance deviation $D$ in Figure 3 shows an even clearer trend, monotonically increasing with triangle area. Both projections have the same maximum $D$ values. The MTP has consistently lower average $D$ values than the CTP; among these triangles, the maximum $D$ for the CTP is about 1.35 to 1.4 times the maximum $D$ for the MTP. The worst distortion, Africa Wall Map's maximum $D$, is less than 5% of its edge lengths, and smaller control triangles have a maximum $D$ that is an even smaller percent.

As true 1:1 scale maps are impractical, absolute values of $s$ are unimportant; the quantity $\sigma = \frac{\max s}{\min s} - 1$ is plotted in Figure 4 instead. The trend of $\sigma$ is less clear. A combination of control triangle area and asymmetry influences this value. In general, this value is higher for MTP than CTP, but not by any consistent factor, and for the large and symmetric Africa Wall Map triangle the MTP is actually lower than the CTP. The amount of scale distortion is small for both; except for the very obtuse Canada Atlas triangle, all values are below 10%.

A comparison of the two projections using the South America Wall Map control points is in Figure 5. The South America Wall Map control triangle is fairly representative, being somewhat asymmetric but not too obtuse. The small part of Central America in the upper left is somewhat shifted between the two maps, as is the western area near Ecuador and Peru, but no features on either map are conspicuously distorted compared to the other. Figure 6 shows ellipses of distortion with centers on a grid at steps of 15° latitude and longitude. Distortion is somewhat more visible in this figure; one can see that the MTP introduces slightly more non-conformal distortion near the control points.

Contour lines of $\omega$ are shown in Figure 7. Those in the CTP are ovals, while those for the MTP extend outward through each edge of the control triangle. Both reach a minimum $\omega$ of 0 at a point inside the control triangle. Highly obtuse control triangles, like Canada Atlas, may have two local minima for $\omega$ within the control triangle. $\omega$

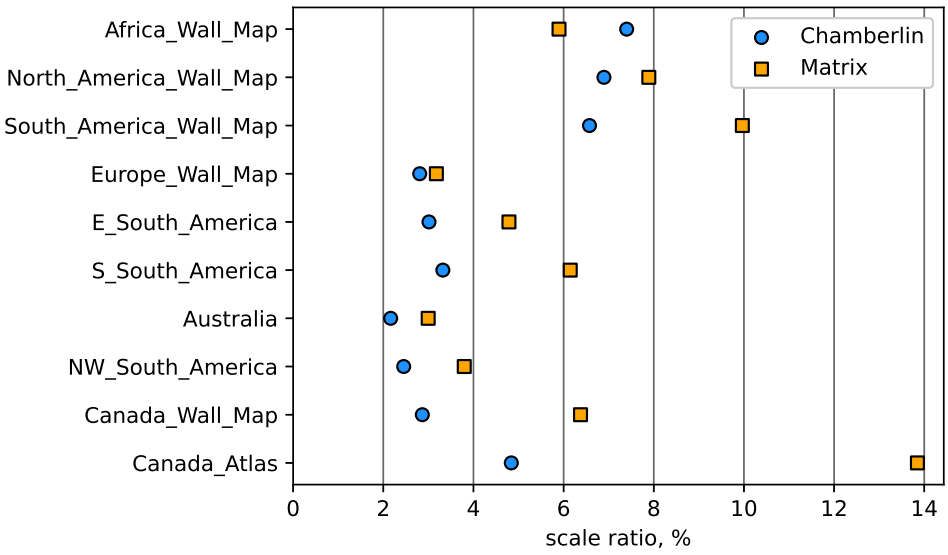


**Figure 4.** Comparison of areal scale ratio $\sigma$.

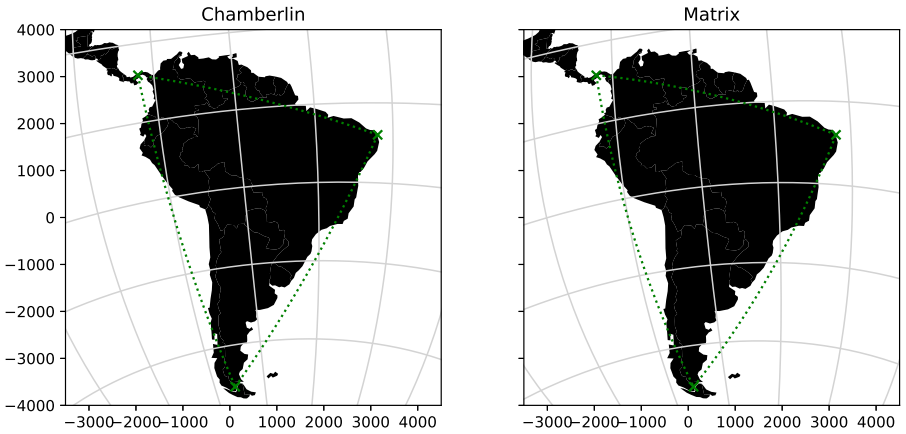


**Figure 5.** Projection of South America and surroundings. Green lines indicate the control triangle and control points in this and the following figures.

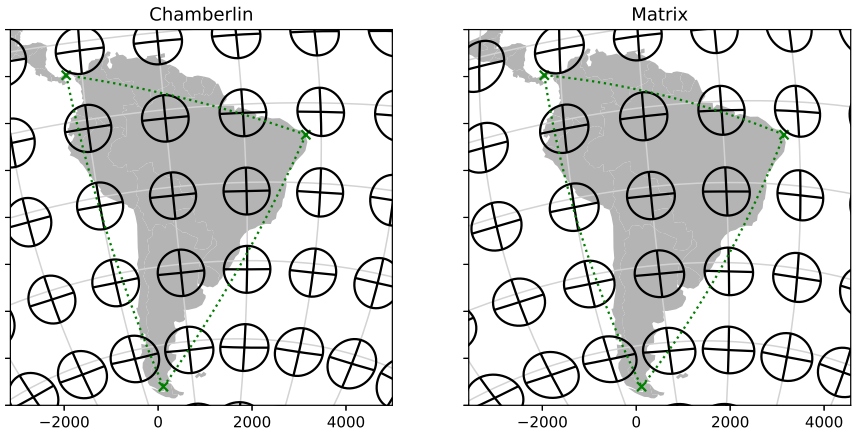


**Figure 6.** Ellipses of distortion, on a 15° grid.

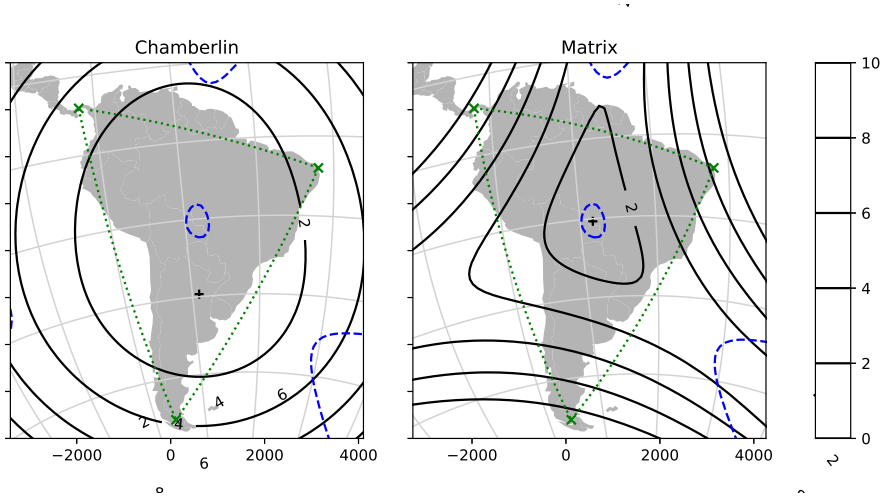


**Figure 7.** Maximum angular deformation $\omega$, in degrees. Blue dashed lines indicate where the two projections have equal $\omega$ values.

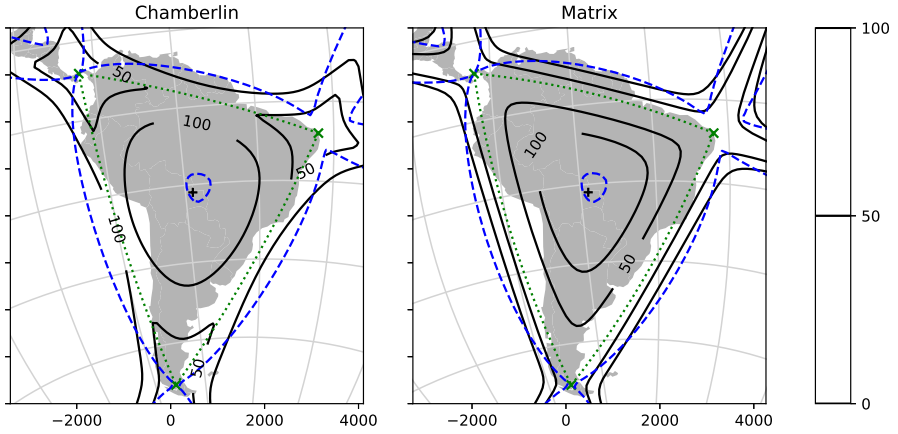


**Figure 8.** Total distance deviation $D$. Blue dashed lines indicate where the two projections have equal $D$ values.

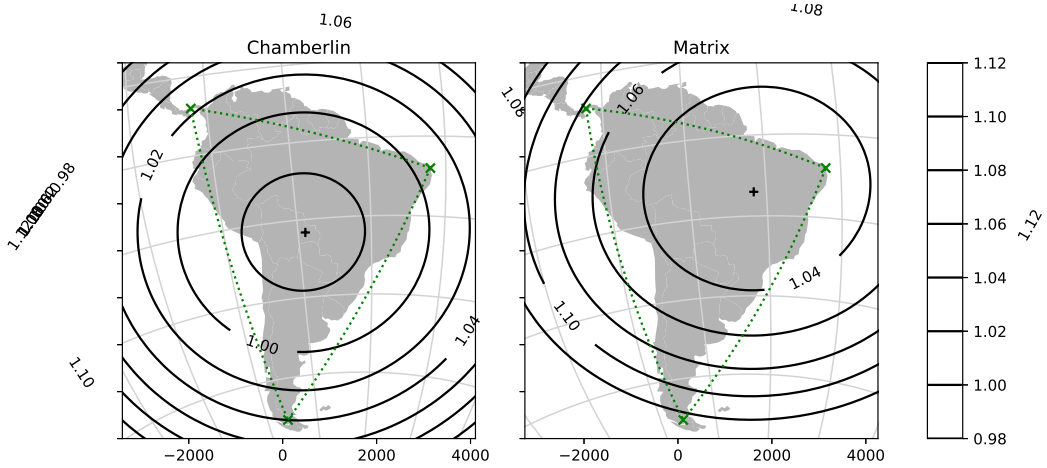


**Figure 9.** Areal scale factor $s$.

is higher for MTP than CTP, except for a small region in the control triangle where both are near 0 and some regions near the boundary of the map.

Figure 8 depicts contour lines of $D$ for these two projections. Both projections have a local minimum of 0 at the control points, which follows from the geometric construction. Both have a local maximum inside the control triangle. $D$ for the MTP is low along the control triangle edges, while for the CTP it is larger. $D$ is lower for MTP than CTP in a region including the control triangle and nearly all of South America, except for a small region near the shared maximum. It is also lower in some regions extending outward from the control points.

Contour lines of $s$ are shown in Figure 9. The contour lines have the same elliptical structure in both projections, centered on a point where $s$ reaches a local minimum. This point is different for each projection, which influences the differences in aggregate area distortion in Figure 4. That minimum value of $s$ is different for each projection.

In most practical applications the area pictured in these figures will be sufficient,

| Projection | Time (s) | Time minus overhead (s) |
|---|---|---|
| CTP | 3.31 | 3.29 |
| MTP | 1.63 | 1.61 |
| No-op | 0.01 | 0.00 |

**Table 2.** Computation time comparison.

but we can state trends as both projections extend outward from the control triangle, outside the area shown in these figures. $\omega$ increases to 180° at the projection boundary, and increases further in the overlap region, representing the inversion there. $D$ increases in general away from the center, but for the MTP $D$ remains low on the great circles containing the control triangle edges. $s$ is bounded for the entire sphere; it increases to a maximum and then decreases to 0 at the projection boundary. If continued into the overlap region, $s$ reaches a negative minimum value.

To determine computation time, the `timeit` package in Python (Van Rossum & Drake, 2009) was used with the PyProj interface to PROJ. (Snow et al., 2020) A data set of 64,800 points across the sphere was projected 100 times. This was done 5 times for each control triangle, and the lowest total time was used, as recommended by the `timeit` documentation. This was done for the two projections and a "no-op" projection that returns the input unchanged, used to estimate overhead. Only the transformation itself was timed, not the initialization of the projection: the initialization time is negligible compared to the time cost of running the projection repeatedly. As expected, the timing differences between control triangles were not significant for either projection, so are not shown here. Table 2 shows the minimum runtimes across all control triangles. Accounting for overhead, the MTP takes slightly less than half the time of the CTP.

## 6. Conclusion

We have demonstrated a new compromise map projection, the matrix trimetric projection (MTP). In general, the differences between the results of the Chamberlin trimetric projection (CTP) and MTP are small enough that either one is adequate for their common use cases. The MTP has the advantage if an inverse is needed, if one wishes to reduce distance distortion, or if processing time is a concern.

The forward formula for the MTP is given in Equations 7–9. Equation 7 is a simple product of a matrix and a vector. The vector depends on the point being transformed. The matrix calculated by the latter two equations depends only on the control points, so can be calculated once and reused. Measuring points transformed per unit time, the MTP is about twice as fast as the CTP. Of course, details of the implementation contribute to the time it takes, but PROJ's implementation of the CTP does not have any obvious inefficiencies and has changed little in more than two decades.

The inverse formula for the MTP is calculated by Equations 10–13 and a single-variable Newton's method iteration using Equations 15 and 16. The matrices in Equations 11 and 12, as well as matrix $\mathbf{A}$ in Equations 15 and 16, also depend only on the control points and can be reused. The CTP, in contrast, has no known inverse aside from brute force two-variable inversion.

Figures 2–4 plot aggregate measures of distortion within each of the listed control triangles. The CTP outperforms the MTP in terms of angular distortion and (except in one case) scale distortion, but the reverse is true for distance distortion. For both

projections, distortion tends to be larger for a larger control triangle. Figures 5–8 show the projections applied to South America, demonstrating the shape of distortions across the mapped area. Differences between the two projections are difficult to see with the eye.

The same control points were used for both projections in this work, but the optimal placement of control points may be somewhat different for the application of different projections to the same geographic feature. The angular distortion of the MTP is lower in a region extending through the middle of the control triangle edges, so one may wish to orient the triangle to take advantage of that.

The MTP is closely related to the CTP. Both are related to the azimuthal equidistant projection and the two-point equidistant projection, which depend on measurements from a single point and from a pair of points, respectively. (Snyder, 1987) This suggests an "$n$-metric" family of projections based on distances from some number of points. The form of the forward formula suggests a possible family of projections that are simple functions of such distances, such as a polynomial function. Additionally, there may exist similar projections using measurements other than distance, such as area.

A software implementation of the MTP, as well as code used to produce the calculations and figures in this text, is available on the author's Github site. (Author, 2020)

## 7. Acknowledgements

Figures in this text were created using the Python packages matplotlib (Hunter, 2007) and GeoPandas (Jordahl et al., 2020), and their dependencies including PROJ (PROJ contributors, 2019) and PyProj (Snow et al., 2020) as referenced earlier. Land mass shape data come from Patterson and Kelso (2020).

## References

Author. (2020). *xxxxxx.* https://github.com/xxxxxxxx/xxxxxxx.

Burden, R., & Faires, J. (2006). Solutions of equations in one variable. In *Numerical analysis* (8.1 ed., pp. 67–85). Cengage Learning.

Christensen, A. H. (1992). The chamberlin trimetric projection. *Cartography and Geographic Information Systems*, *19*(2), 88-100.

Hunter, J. D. (2007). Matplotlib: A 2d graphics environment. *Computing in Science Engineering*, *9*(3), 90-95.

Isaacs, I. (2009). Triangles. In *Geometry for college students* (pp. 50–93). American Mathematical Society.

Jordahl, K., den Bossche, J. V., Fleischmann, M., Wasserman, J., McBride, J., Gerard, J., ... Leblanc, F. (2020). *geopandas/geopandas: v0.8.1.* https://zenodo.org/record/3946761. Zenodo.

Lapaine, M. (2017). Modelling the world. In A. Kent & P. Vujakovic (Eds.), *The Routledge handbook of mapping and cartography* (pp. 187–201). Taylor & Francis.

Patterson, T., & Kelso, N. V. (2020). *Natural earth.* https://www.naturalearthdata.com/. (Accessed: 2020-01-17)

Posamentier, A., & Salkind, C. (1996). The Pythagorean theorem. In *Challenging problems in geometry* (pp. 85–86). Dover Publications.

PROJ contributors. (2019). PROJ coordinate transformation software library [Computer software manual]. Retrieved from `https://proj.org/`

Snow, A. D., Whitaker, J., Cochran, M., den Bossche, J. V., Mayo, C., de Kloe, J., ... Taves, M. (2020, November). *pyproj4/pyproj: 3.0.0.* Zenodo. Retrieved from `https://doi.org/10.5281/zenodo.4247339`

Snyder, J. P. (1987). *Map projections–a working manual* (No. 1395). US Government Printing Office.

Strang, G. (1980). *Linear algebra and its applications.* Academic Press.

Van Rossum, G., & Drake, F. L. (2009). *Python 3 reference manual.* Scotts Valley, CA: CreateSpace.

Wohlgemuth, M. (2010). Ein Satz von Carnot. In *Mathematisch für fortgeschrittene Anfänger: Weitere beliebte Beiträge von Matroids Matheplanet* (pp. 273–276). Spektrum Akademischer Verlag.